

Original Article

Cite this article: Meyers T, Alsbou N, Ahmad S, and Ali I. (2025) A four-dimensional dosimeter and quality assurance phantom to quantify respiratory motion effects on the dose delivery for adaptive radiation therapy. *Journal of Radiotherapy in Practice*. 24(e2), 1–9. doi: [10.1017/S1460396924000359](https://doi.org/10.1017/S1460396924000359)

Received: 27 August 2024

Revised: 22 November 2024

Accepted: 16 December 2024


Keywords:

Adaptive radiation therapy; reparatory motion; 4D dose calculation; 4D dosimeter

Corresponding author:

Imad Ali; Email: imad-ali@ouhsc.edu

A four-dimensional dosimeter and quality assurance phantom to quantify respiratory motion effects on the dose delivery for adaptive radiation therapy

Taylor Meyers¹, Nesreen Alsbou², Salahuddin Ahmad³ and Imad Ali³ 

¹Radiation Oncology, MD Anderson Cancer Center, 7675 Phoenix Dr, Houston, TX 77030, USA; ²School of Engineering and Physics, Howell Hall 221R, University of Central Oklahoma, Edmond, OK 73034, USA and ³Department of Radiation Oncology, University of Oklahoma Health Sciences Center, 800 N.E. 10th Street, OKCC L100, Oklahoma City, OK 73104, USA

Abstract

Purpose: A 4D-dosimeter and quality assurance phantom prototype was developed to quantify the effects of respiratory motion.

Methods: The dose distributions were measured using two-dimensional detectors that were mounted on a mobile platform capable of sinusoidal motion in one direction with different patterns using adjustable motion amplitude and frequency. The dose distributions were obtained from various treatment plans including conformal and intensity-modulated beams for both photon and proton therapy. Dose delivery and measurement were conducted using this 4D-dosimeter with the mobile phantom for different motion amplitudes (0–35 mm) and frequencies (0.25–0.33 Hz).

Results: The increase in motion amplitude increased the blurring of the dose distributions at the beam edges along the direction of motion and led to large dose discrepancies. This produced larger dose deficits inside the treatment planning volume (PTV) and increasing dose deposition in the surrounding normal tissue with increasing motion amplitudes. For both the IMRT and VMAT-treatment plans, the dose profile for each increased amplitude increment showed a reproducible flattening of the penumbra at the beam edge, all changing around the 40–60% isodose line.

Conclusion: The 4D-dosimeter developed in this work provides a noble clinical tool to quantify the deviations in the dose distributions induced by respiratory motion.

Introduction

Patient-specific intensity-modulated radiation therapy (IMRT), volumetric-modulated arc therapy (VMAT) and intensity-modulated proton therapy (IMPT) quality assurance protocols should be implemented in the clinic prior to treatment of the patients¹. This typically involves the verification of the dose distributions calculated by the treatment planning system by measurement using quality assurance dosimeters and phantoms. The treatment plans with the dose calculation and optimisation parameters are transferred from the patient CT images to the CT images of a quality assurance phantom. Then, the dose distributions are calculated on the quality assurance phantom and delivered on the machine. The measured and calculated dose distributions on the quality assurance phantom are compared to determine the dose difference, distance-to-agreement and gamma index². Most current quality assurance protocols apply a treatment plan optimised and calculated in 3D on a phantom where the calculated and measured dose distribution are performed under static conditions. These quality assurance procedures are usually used to verify dosimetric accuracy of the dose distributions calculated by the treatment planning system. These methods of using stationary phantoms do not accurately consider patient motion that affects patients treated with radiation therapy at the different stages of the procedure including CT imaging and simulation, treatment planning and dose delivery^{3,4}. Furthermore, these protocols fail to consider the effects of intra- and inter-fractional motion on the dose distribution that are actually received by the mobile patients during the radiation therapy course^{5,6}.

Patient motion can be caused by the skeletal-muscular, cardiac, gastrointestinal and respiratory systems. Respiratory motion particularly remains one of the forefront challenges towards motion management in radiation therapy because breathing can affect different treatment sites such as lungs, oesophagus, liver, pancreas, breast and prostate⁷. Patient motion can lead to large deviations in the dose coverage of the tumour and sparing of the normal tissue expected from the optimised treatment plans⁸. It is important to consider patient motion when performing quality assurance and dose verification on patient treatment plans to accurately simulate patient conditions during

© The Author(s), 2025. Published by Cambridge University Press. This is an Open Access article, distributed under the terms of the Creative Commons Attribution licence (<https://creativecommons.org/licenses/by/4.0/>), which permits unrestricted re-use, distribution and reproduction, provided the original article is properly cited.

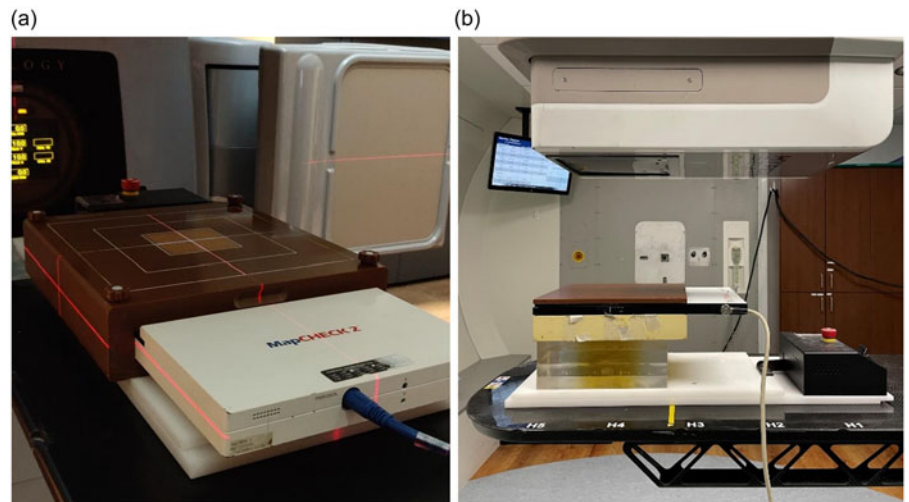


Figure 1. Experimental set-up of the (a) Mapcheck2 phantom aligned at isocentre of a Varian Trilogy Linac and (b) Octavius729XDR phantom aligned at isocentre of a MEVION = S250i HYPERSCAN proton system. Both systems were mounted on the top of a motion platform.

therapy. Many studies have been conducted that attempt to introduce an anthropomorphic motion phantoms which have the capabilities of modelling the complex patterns of patient's respiratory motion^{9–11}. **The aims of this study include investigating the effects of respiratory motion on the delivered dose distributions for different treatment plans that include conformal, IMRT, VMAT and IMPT produced for the treatment of different sites to quantify underdosing of the tumour and overdosing of the normal surrounding tissues. Furthermore, the effects of variations in motion amplitude and frequency on the dose distributions that were optimised in 3D on static CT images using current dose calculation algorithms used for treatment planning were quantified.**

Materials and Methods

Treatment planning

In this study, various 3D-optimised treatment plans using conformal beam, IMRT, VMAT and IMPT were delivered to a 2D detectors placed on a motion platform (Standard Imaging Inc, Middleton, WI). The mobile platform moved in one dimension sinusoidally producing different motion patterns with adjustable amplitude and frequency. The MapCheck2 phantom (Sun Nuclear, Melbourne, FL) made from multiple array diodes was used to measure the dose distributions for the conformal, IMRT and VMAT treatment plans delivered by a Varian Trilogy and Truebeam-STX Linear Accelerators (Varian Medical Systems, Inc., Palo Alto, CA)¹². The OCTAVIUS phantom (PTW, Freiburg, GmbH) made from 2D multiple array ionisation chambers was used to measure the dose distributions for the IMPT treatment plans delivered by the Mevion-S250i HYPERSCAN proton system (MEVION Medical Systems, Littleton, MA, USA)^{13,14}. The treatment plans 10 in total represented different treatment sites of head and neck, thorax, abdomen, and pelvis. The plans were first delivered for a static condition which was used as a reference representing typical conditions for patient-specific quality assurance testing. Then, it was followed by dose delivery with the mobile platform which moved at amplitudes in the range 0–35 mm using frequencies of 0.2–0.33 Hz. The mobile phantom was placed on the treatment couch where different sinusoidal motion patterns were

applied in the superior–inferior direction during beam delivery as shown in Figure 1.

The 2D dose distributions from the photon plans were measured with a multiple-diode array MapCheck2 phantom which consisted of 1,527 diodes arranged in arrays that are offset by 5 mm as shown in Figure 1a¹⁵. The overall effective detection area of the detector is 32×26 cm² with an array geometry of 10 mm detector spacing parallel to the X- and Y-axis and row spacing of 5 mm. The minimal distance between the centre of the detectors was uniform throughout the array at 7.07 mm. The active single detector area and volume were 0.64 mm² and 0.019 mm³, respectively. The diodes were located at 12 mm depth within the phantom, which was equivalent to 20 mm of solid water build-up. The diodes were encapsulated with an additional 3 cm of solid water on the top to provide sufficient depth for dose measurement mimicking tumour depths and eliminating dose artefacts in the build-up region and electron contaminations. Another 3 cm phantom was layered beneath the detector to eliminate backscatter issues. The dose distributions for the IMPT plans were measured using the OCTAVIUS Detector 729XDR^{16,17}, which was made from a multiple-array ion chamber matrix commonly used for quality control and patient plan verification using protons or heavy ions. This detector, shown in Figure 1b, consisted of 729 vented plane-parallel ion chambers arranged in an effective detection area of 27×27 cm². The size of each vented plane-parallel ion chamber is 5×5×3 mm³, and they were aligned in rows and columns with a separation of 10 mm. In contrast to the diodes, ion chambers were more resilient to the damage from the neutrons that were produced from the interaction of the proton beam. The treatment plans were mapped on the OCTAVIUS detector encapsulated in phantom with different thicknesses to simulate the tumour depth in the patient-specific plans for proper dose verification of the spread-out Bragg peak, the proximal and distal ranges of the proton beams calculated by the treatment planning system. **The 2D dose distributions from the photon and proton plans measured with mobile phantom were compared with the corresponding dose distributions measured with the stationary phantom. Different dosimetric parameters that included dose difference, dose deficit in the tumour, dose spread-out and the gamma index were calculated to quantify the effect of phantom motion on the dose distributions.**

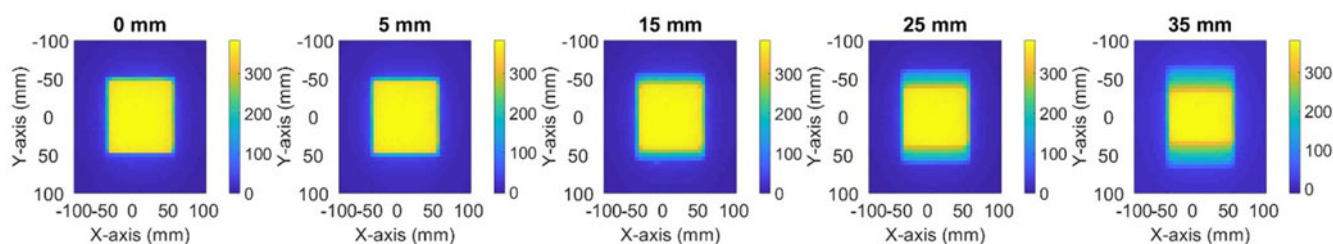


Figure 2. 2D dose distributions for 10×10 cm² open fields with motion amplitudes of 0, 5, 15, 25 and 35 mm at 3 sec/cycle. The colour bar represents the dose level in cGy.

Results

Dose distributions dependence on motion amplitude

Conformal plans with open fields

The variations of the 2D dose distributions **from open fields** with motion amplitudes ranging 0–35 mm at a constant cycle interval of 3 s is shown in Figure 2. As the motion amplitude increased, the spread-out of the dose distributions at the beam edge increased. The extent of the dose spread-out correlated with the motion amplitude, with the edge blurring equating to half the motion amplitude from each side of the dose distributions along the direction of motion.

Figure 3a shows the dose profiles normalised to the central axis dose (100%) for the 10×10 cm² open field along the direction of motion (Y-axis). While Figure 3b shows the percent dose difference of the mobile dose distribution relative to the static dose distribution for the motion amplitudes 5–35 mm. For the static condition, the penumbra showed a sharp dose fall-off at the beam edge indicating the dose distributions from conformal fields. As the motion amplitude increased, the penumbra experienced a spread-out about the 50% isodose line that caused the beam edge to broaden. With increasing motion amplitude, the region inside the treatment volume experienced underdosing, while the region outside of the treatment volume experienced overdosing. The spread-out of this region on one edge of the dose profile, from the overdosing outside the volume and underdosing inside the volume, was approximately half the size of the motion amplitude. The magnitudes of the overdosing and underdosing regions were further investigated quantitatively in Figure 3, with the smallest motion amplitude of 5 mm yielded an overdosing of 40% outside the treatment volume and underdosing of 20% inside the treatment volume. While the largest motion amplitude of 35 mm produced an overdose of approximately 75% in the surrounding normal tissue and an underdosing of nearly 60% within the treatment volume. For this conformal plan that delivered a flat uniform dose, the central region of the beam remained unchanged for all mobile conditions for the range of motion amplitudes (0–35 mm) used in this study. This may change for small fields with their length equal to the motion amplitudes.

IMRT-optimised plans

Figure 4(a, b, c, d) shows the 2D dose distributions for IMRT plans for different treatment sites that include: (a) head and neck, (b) lung, (c) abdomen and (d) pelvis. The dose distributions were displayed with increasing motion amplitude, beginning with the static condition and then increasing in motion amplitude from 5 mm to 35 mm. Similar to the open field, the dose distributions were spread out at the beam edge along the direction of motion which increased as the motion amplitude increased.

Similar behaviour was noted in the normalised dose profiles of the different IMRT plans for the different treatment sites as shown in Figure 5a. The dose distributions spread out with an overdosing outside the treatment volume and underdosing inside the treatment volume. The spread-out in the penumbra regions increased as the motion amplitude increased; however, it depended on the local dose peaks of each IMRT dose profile for the different treatment plans. Furthermore, the motion artefacts also induced variations in the local doses and the dose distributions inside the PTV. The right column in Figure 5(b, d, f, h) showed percentage dose differences of underdosing in the tumour and overdosing in the surrounding tissues relative to the static dose distributions which were optimised without consideration of patient motion. The spread-out of the dose distributions from the IMRT plans produced similar effects with increasing severity as the amplitude increased. In most cases, the smallest motion amplitude of 5 mm used in this study resulted underdosing inside the treatment volume by 5–20% and overdosing of 20–30% in the surrounding tissues. While the largest motion amplitude of 35 mm resulted in underdosing from 40 to 60% inside the treatment volume and overdosing from 60–80% in the nearby tissues.

VMAT-optimised plans

Figure 6 shows the 2D dose distributions obtained from a (a) Head and Neck, (b) Lung and (c) Abdomen VMAT plans delivered by a Varian TrueBeam linear accelerator. The measured dose distributions for the VMAT plans showed similar behaviour to those obtained for the IMRT plans where the spread-out at the beam edges increased along the direction of the motion with increasing motion amplitude from 0 to 35 mm as shown in Figure 7. However, the dose deviations from the motion artefacts were more pronounced inside the tumour as shown in figure. This resulted from several factors that include increased intensity modulation, rotation of the gantry around the patient and cross-talking between the phantom motion, MLC-motion and gantry motion in the VMAT plans.

IMPT-optimised plans

Figure 8 shows the 2D dose distributions of a left breast treatment plan using the MEVION-S250i proton system for motion amplitudes ranging 0–35 mm. The dose spread-out at the beam edge increased with increasing motion amplitude similar to the IMRT and VMAT photon plans. However, the dose distributions from the spot scanning proton beam within the tumour were distorted substantially by motion. The flat dose regions and local dose distributions in the proton plans changed within the tumour depending on the motion amplitude due to substantial cross-talking effect of the scanning proton spot beam with the phantom motion. Figure 8a shows the normalised percentage dose profiles

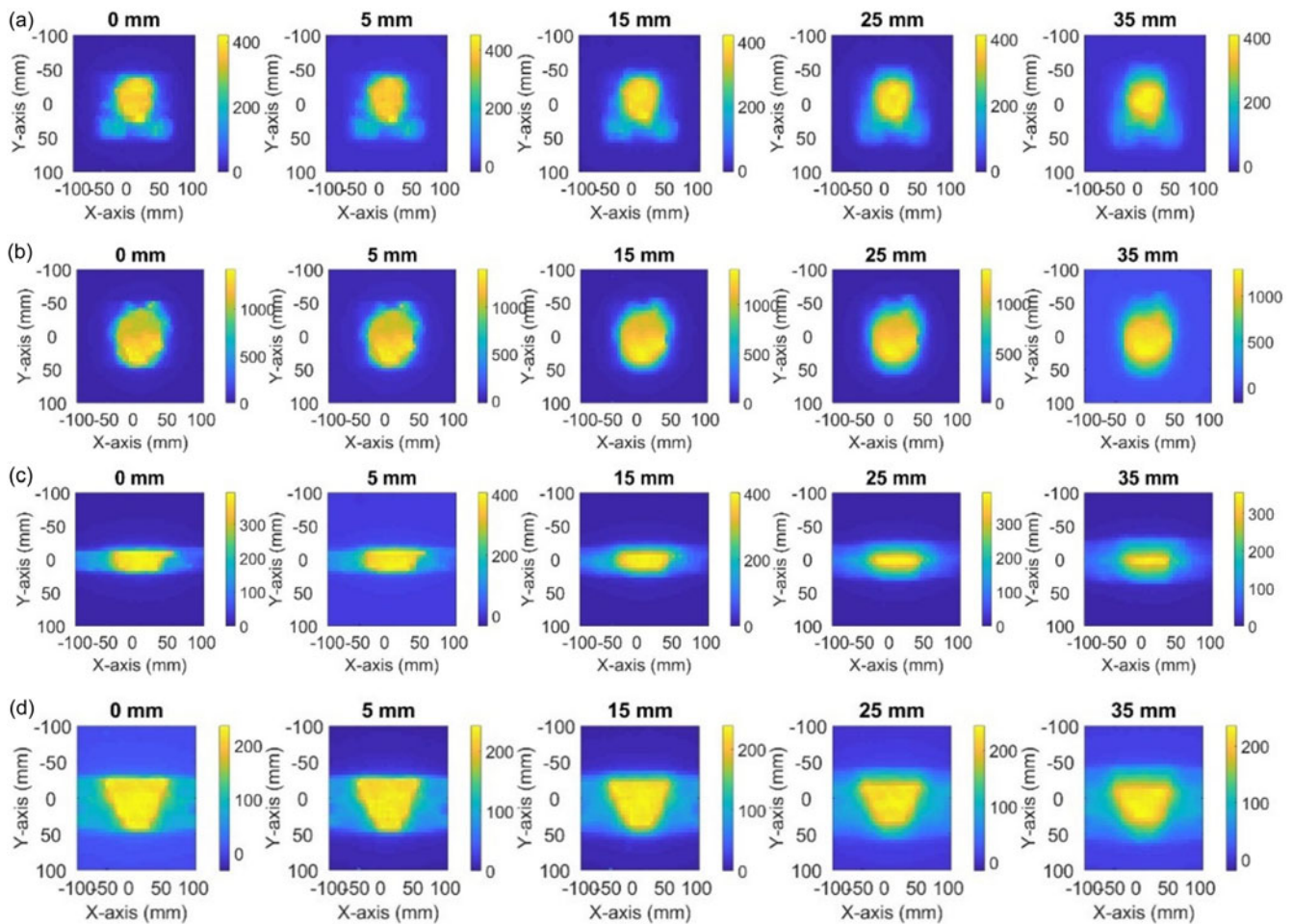
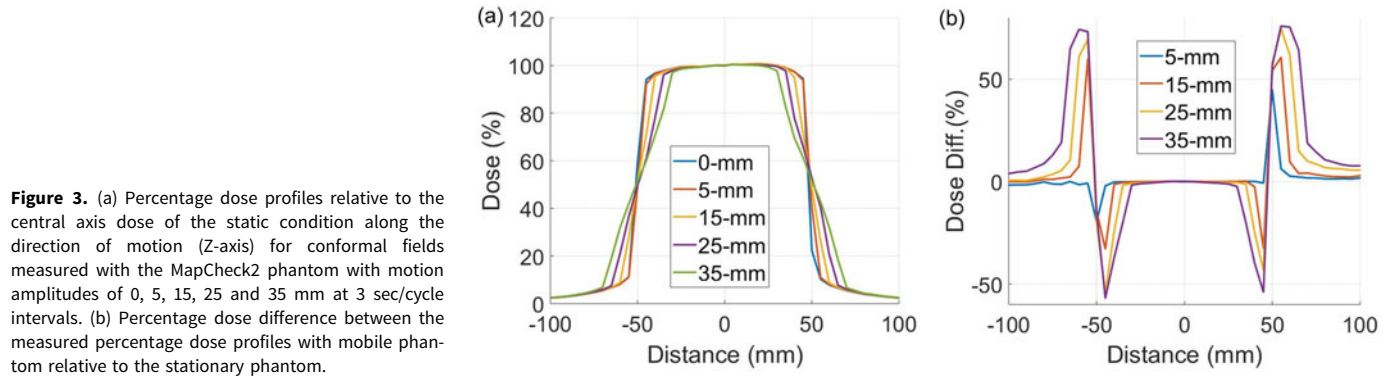


Figure 4. 2D dose distributions measured with the MapCheck2 phantom for (a) head and neck, (b) lung, (c) abdomen and (d) pelvis IMRT patient treatment plans with motion amplitudes of 0, 5, 15, 25 and 35 mm at 3 sec/cycle. The colour bar represents the dose level in cGy.

normalised to the central axis dose acquired with the static phantom. The motion effects close to the penumbra for the proton plan did not follow similar behaviour as seen in the previous IMRT and VMAT treatment plans. While the photon dose distributions showed spread-out for all motion amplitudes around the 50% dose point along the direction of motion, there was no systematic blurring of the dose distributions around the 50% point for the dose distributions from the spot scanning proton beams. In addition, the central region of the dose distributions of the proton plans deviated significantly with the different motion amplitudes,

which resulted displacement of the hot spots within the treatment volume. The central region of the fields showed non-uniform percent differences between each motion amplitude as shown in Figure 8c. While the dose close to the central axis in the IMRT and VMAT plans deviated from 0–5%, the IMPT plans central doses deviated by up to 50% for large motion amplitudes as shown in Figure 9a,b. The large deviations in the dose distribution close to the penumbra and near the central axis regions resulted from the complex interplay effects between the proton spot scanning beam and the phantom motion. As the proton delivery system used a

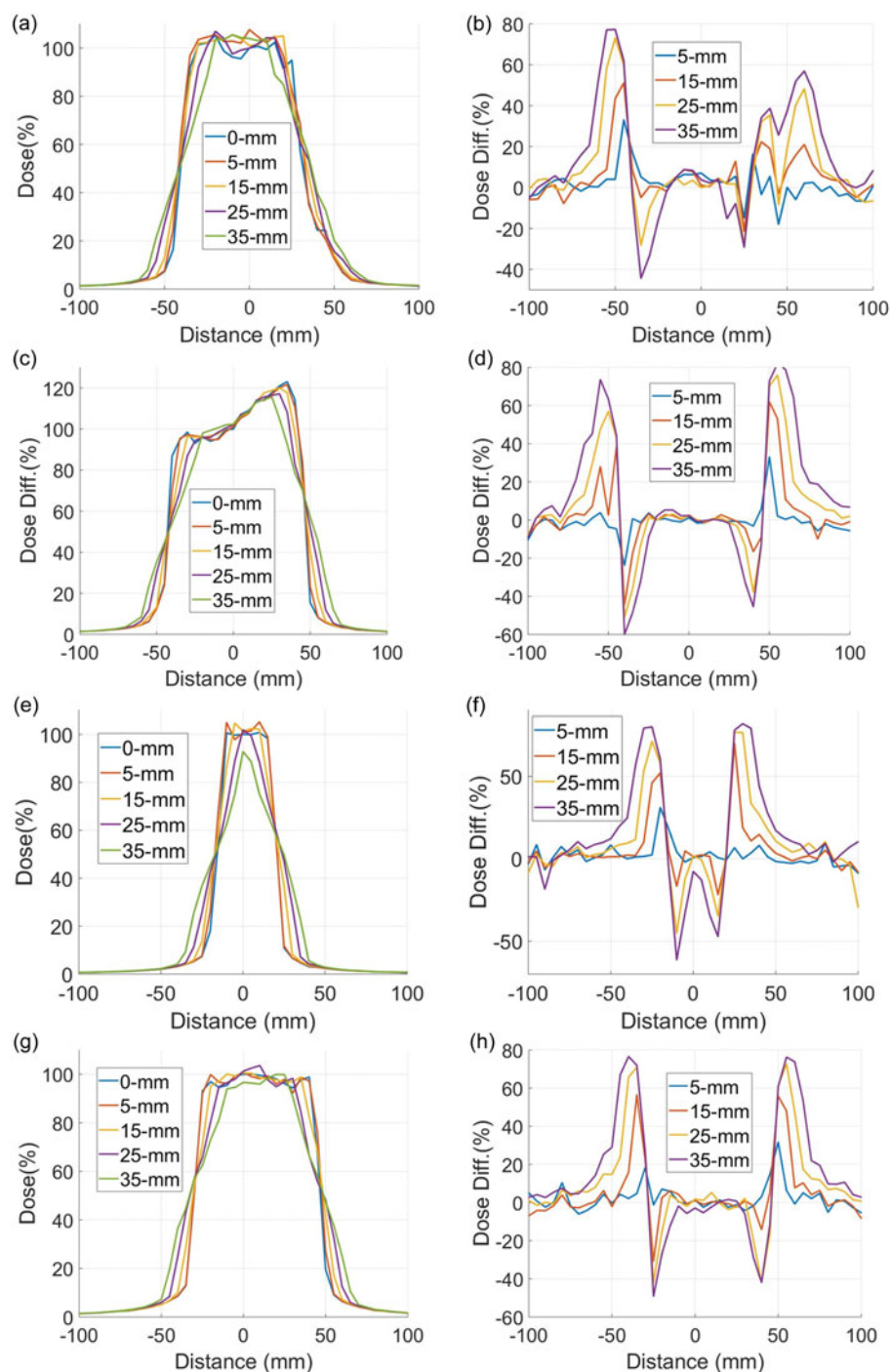


Figure 5. The figures in the left column represent the percentage dose profiles normalised to the central axis dose (100%) measured with mobile phantom relative to the dose profile measured with static condition along the direction of motion for (a–b) Head and Neck, (c–d) Lung, (e–f) Abdomen and (g–h) Pelvis IMRT plans for motion amplitudes of 0, 5, 15, 25 and 35 mm at 3 sec/cycle intervals. The figures in the right column show the corresponding percentage dose difference of the mobile relative to the static phantom.

scanning pencil beam and not a flat field of variable intensity produced by the linear accelerators, the dose delivered by the spot scanning pencil beam would vary depending on its overlap with the phantom motion cycle.

Dose distributions dependence on cycle interval

Figure 10 shows the variations of the dose distributions delivered motion cycle intervals of 2 sec/cycle and 6 sec/cycle. Small changes in the dose profiles were measured with two motion cycle intervals for both motion amplitudes of 5 and 35 mm. The percentage dose deviations between the two cycle intervals were

within 3% as shown in Figure 10c. The dose differences were nearly 5% at the field edge due to spatial mismatching of the dose profiles because of the uncertainty in the detector positioning during measurement.

Quality assurance testing: Gamma Index

Figure 11 shows the gamma index passing rates with a criterion of 3%/3 mm calculated for different IMRT and VMAT plans with motion amplitudes 3–35 mm that were used on the mobile phantom. The gamma test was calculated using the dose distributions recorded with the different motion amplitudes relative

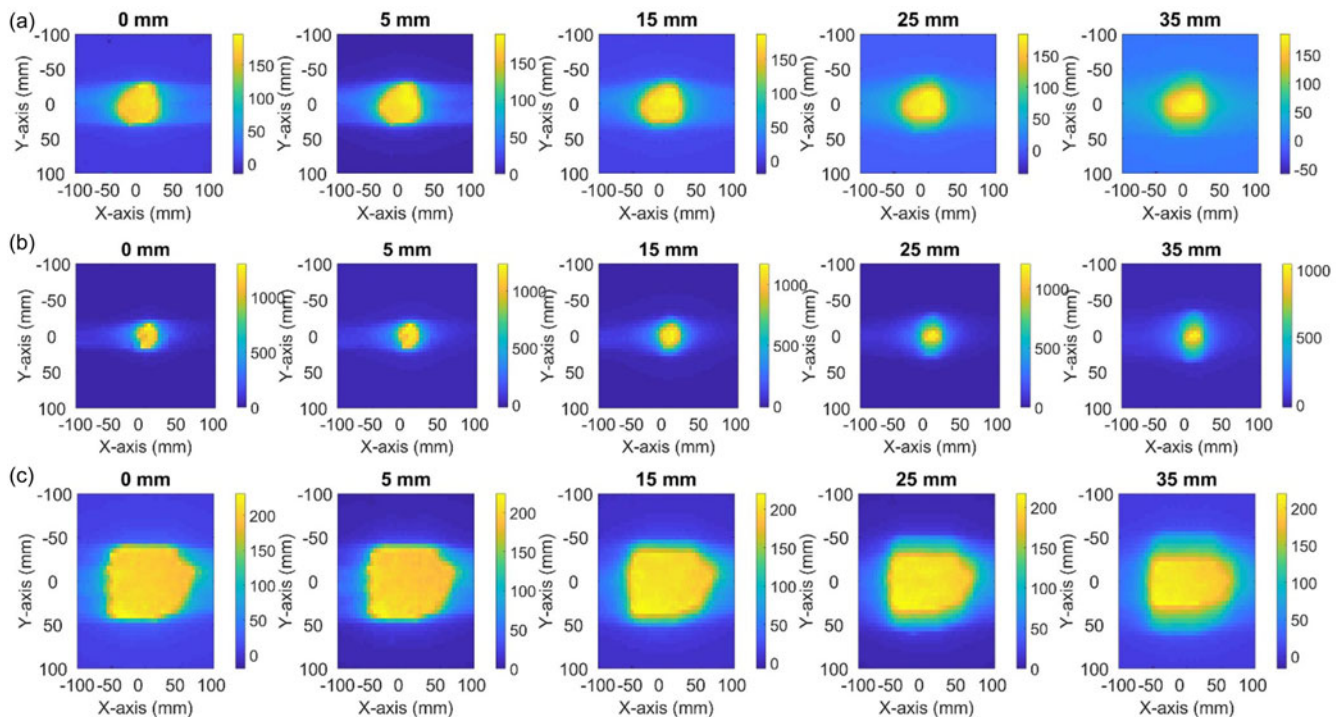


Figure 6. 2D dose distributions of VMAT for (a) Head and Neck, (b) Lung and (c) Abdomen plans measured with the MapCheck2 phantom with motion amplitudes of 0, 5, 15, 25 and 35 mm at 3 sec/cycle. The colour bar represents the dose level in cGy.

to that recorded under static conditions. The gamma passing rate decreased as the motion amplitude increased because of the deviations introduced by motion artefacts. The decline in the gamma passing rates were more significant for the IMRT plans compared to that of the VMAT plans which was due to the shorter delivery time of the VMAT plans that resulted less motion artefacts.

Discussion

The combination of the 2D detectors including the MapCheck2 or OCTAVIUS with the mobile phantom set-up provided this 4D dosimetric system that was used to quantify the discrepancies induced by respiratory motion on conformal, IMRT, VMAT and IMPT plans. These dose discrepancies mimic the deviations between the dose distributions obtained from 3D-optimised plans using static CT imaging and the actual delivered dose distributions with patient breathing. The dose distributions of the mobile phantom spread outside the tumour volume with reproducible characteristics of underdosing of the tumour and overdosing of the surrounding area **as indicated by other studies**^{18,19}. These artefacts are not accounted for in treatment plans that do not consider the respiratory motion in the treatment planning and dose delivery processes. The 4D dosimeter developed in this work provides a novel tool to quantify the dose deviation induced by respiratory motion **compared with previous studies**^{20–23}. Innovative dosimetric tools have to be developed to measure motion artefact, and new approaches are needed to account for these dose artefacts in the treatment planning, quality assurance and dose delivery techniques to ensure accurate dose delivery.

The conformal plans showed systematic spread-out of the dose distributions around the 50% isodose line along the direction of motion with a flat dose near the central axis **as indicated by previous studies**^{24,25}. However, the IMRT and VMAT plans showed

large variations in the dose distributions overall including the tumour volume because of shifts in the local doses due to the phantom motion. The features of the dose distributions were consistent in the treatment plans for IMRT and VMAT with photon beams. However, different patterns were produced noticeably in the proton IMPT plans by motion artefacts **as reported in previous studies**^{26,27}. While the conformal, IMRT and VMAT spread-out systematically around a single point where the 50% isodose line with increasing motion amplitude, the dose patterns were not reliably reproducible or predictable in the IMPT plans. In addition, the location of the peak doses or hot spots within the central region of the treatment volume varied significantly in the measured dose distribution of the proton plans compared to photon plans. This resulted because the dose from the photon beams were delivered uniformly over the tumour volume and the overall dose in the central region averaged out, while in the IMPT plan the dose was delivered by a scanning pencil beam locally in one region and gradually until the dose coverage of the entire volume was achieved. The proton dose delivery method was subject to larger interplay effects with the mobile phantom, where the location of the phantom voxels changed constantly during dose delivery with spot scanning proton beam. This resulted in large dose variations ranging from 10 to 20% in the central region of the dose distribution in the proton plan compared to just 0–5% the photon dose distributions due to motion artefacts. One limitation of this study is the use of treatment plans with intermediate to large PTV, where the treatment beams were larger than the motion amplitudes (5–35 mm) used. We expect that the use of treatment plans for small targets comparable or smaller than the motion amplitudes will induce more substantial artefacts in the dose distributions measured with this 4D dosimeter.

While the variations in motion amplitude resulted in large deviations in the dose distributions with the mobile phantom relative to stationary, the variations in the motion frequency did

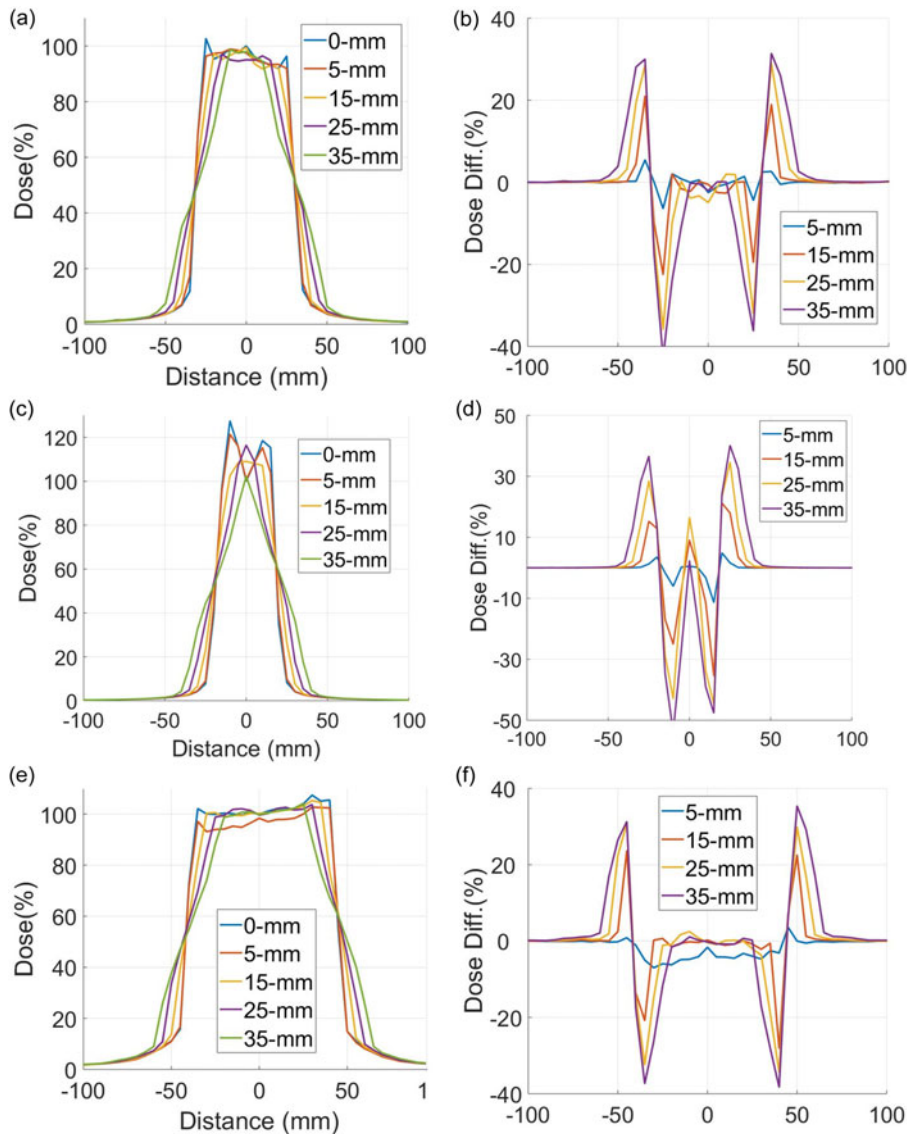


Figure 7. The figures in the left column show the percentage dose profiles normalised to the central axis dose of mobile profiles relative to the static profiles measured with the MapCheck2 phantom along the direction of motion (Y-axis) for (a) Head and Neck, (c) Lung and (e) Abdomen VMAT plans for motion amplitudes of 0, 5, 15, 25 and 35 mm at 3 sec/cycle intervals. The figures in the right column show the corresponding percentage dose differences of the mobile relative to the static profiles.

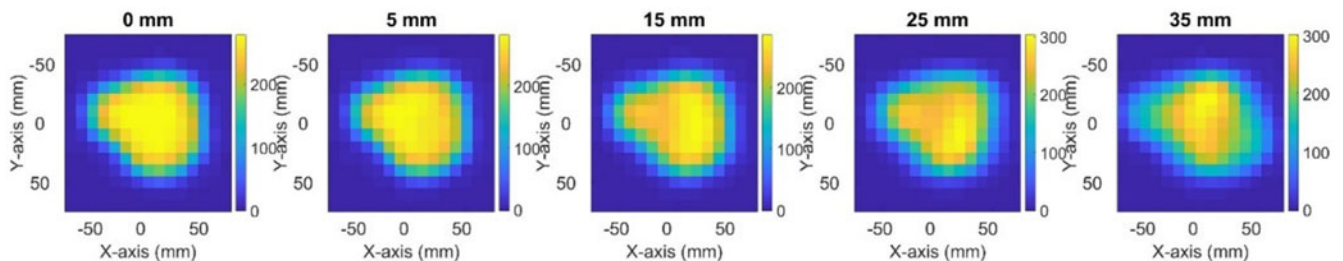


Figure 8. 2D dose distribution measured with the OCTAVIUS 729XDR phantom for a left breast IMPT plan with different motion amplitudes of 0, 5, 15, 25 and 35 mm at 3 sec/cycle. The colour bar represent the dose level in cGy.

not result in substantial dose effects. This can be explained by dose averaging effects due to elongated dose delivery on the machine (nearly 60 sec per beam) in comparison with the motion frequency (3–4 sec cycles), where the dose delivery occurred over multiple motion cycles and the dose rates were too low for the motion frequency to have considerable effects. Another limitation of this study is the use of large cumulative doses

with relatively low dose rates. The motion frequency might strongly affect the dose distributions delivered with high dose rates over short time periods comparable to the periods of the respiratory cycle. Further investigation is required using treatment plans with higher dose rates to quantify the effects that motion frequency may have on dose distributions in future studies. The gamma index analysis of IMRT and VMAT treatment plans

Figure 9. (a) Percentage dose profile normalised to the central axis dose of the static condition along the direction of motion (Z-axis), and (b) the percentage dose difference of each mobile condition relative to the static condition.

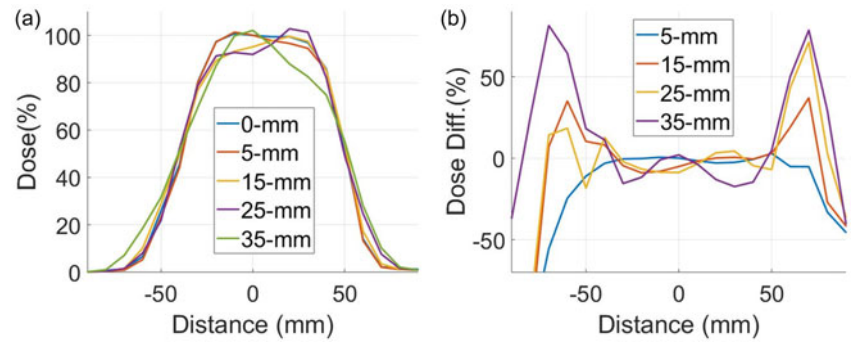


Figure 10. Normalised dose profiles for a VMAT lung plan for motion frequencies of 2 sec/cycle relative to 6 sec/cycle using (a) 5 mm motion amplitude and (b) 35 mm motion amplitude. (c) The percentage dose difference between the two cycle intervals for both the 5 mm and 35 mm motion amplitudes.

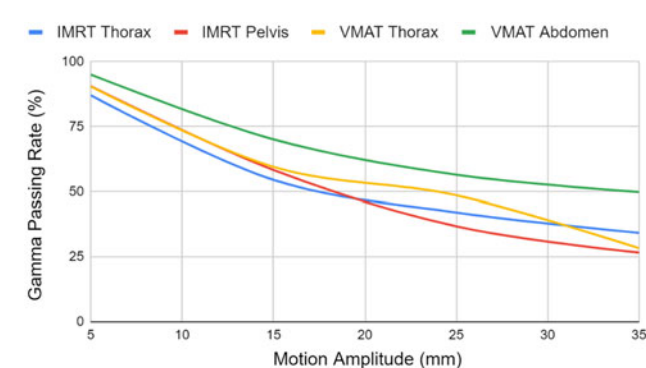
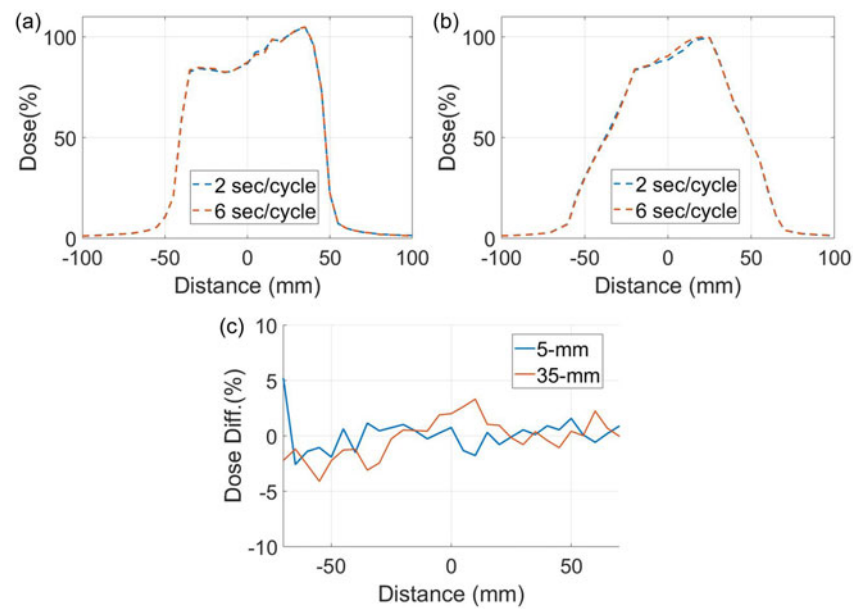


Figure 11. Gamma index passing rate using criterion of 3%/3 mm as a function of motion amplitude 5–35 mm for lung and pelvis IMRT plans and lung and abdomen VMAT plans.

showed a steady decline in passing rates as the range of motion applied on the phantom increased, indicating the importance of motion management techniques for accurate dose delivery and quality assurance of patient-specific treatment plans to consider motion artefacts. The dose spread-out for the photon plans was reproducible and could be modelled for the cyclic motion of the mobile phantom system. These features can be employed to develop motion management techniques for adaptive radiation

therapy and dose calculation algorithms with capabilities to perform 4D optimisation of the treatment plans that can account for motion in real time with new innovative techniques that can be developed in the future^{28,29}.

Conclusion

Phantom motion caused significant variations in the dose distributions measured for conformal, IMRT, VMAT and IMPT plans. The motion artefact increased with increasing motion amplitude, and it was more prominent in proton plans compared to photon plans. The dose distributions in all cases showed spread-out effects at the beam edge and changes in the local dose distribution in the tumour which were simulated for varying motion amplitudes and frequencies. **The measured dose distributions with this mobile phantom provided a quantitative characterisation of the changes in the dose distributions induced by sinusoidal motion that simulated respiratory motion of cancer patients treated with radiation therapy. The 4D dosimeter developed and tested in this work provided a prototype of a noble quality assurance system that can be used to quantify dose deviations induced by respiratory motion that were present during dose delivery for actual patients. It is also a superior tool that can be used for quality assurance and dose verification of futuristic 4D dose optimisation and calculation algorithms that aim to compensate for respiratory motion**

effects in order to provide conformal dose distributions and achieve the goals of adaptive radiation therapy.

Acknowledgements. None.

Financial support. This research was not funded by grant money.

Competing interests. The authors declare no competing interests related to this study.

References

1. Agazaryan N, Solberg TD, DeMarco JJ. Patient specific quality assurance for the delivery of intensity modulated radiotherapy. *J Appl Clin Med Phys* 2003; 4: 40–50.
2. Low DA, Harms WB, Mutic S, Purdy JA. A technique for the quantitative evaluation of dose distributions. *Med Phys* 1998; 25: 656–661.
3. Ali I, Alsbou N, Algan O, Herman T, Ahmad S. Quantitative assessment by measurement and modeling of mobile target elongation in cone-beam computed tomographic imaging. *J Appl Clin Med Phys* 2014; 15: 266–274.
4. Bernatowicz K, Keall P, Mishra P, Knopf A, Lomax A, Kipritidis J. Quantifying the impact of respiratory-gated 4D CT acquisition on thoracic image quality: a digital phantom study. *Med Phys* 2015; 42: 324–334.
5. Yang B, Geng H, Ding Y, Kong CW, Cheung CW, Chiu TL, Lam WW, Cheung KY, Yu SK. Development of a novel methodology for QA of respiratory-gated and VMAT beam delivery using Octavius 4D phantom. *Med Dosim* 2019; 44: 83–90.
6. Giraud P, Morvan E, Claude L, Mornex F, Le Pechoux C, Bachaud JM, Boisselier P, Beckendorf V, Morelle M, Carrere MO. Respiratory gating techniques for optimization of lung cancer radiotherapy. *J Thorac Oncol* 2011; 6: 2058–2068.
7. Keall P, Mageras GS, Balter JM, Emery RS, Forster KM, Jiang SB, Kapatoes JM, Low DA, Murphy MJ, Murray BR, Ramsey CR, Van Herk MB, Vedam SS, Wong JW, Yorke E. The management of respiratory motion in radiation oncology report of AAPM Task Group 76. *Med Phys* 2006; 33: 3874–3900.
8. Mageras GS, Yorke E. Deep inspiration breath hold and respiratory gating strategies for reducing organ motion in radiation treatment. *Semin Radiat Oncol* 2004; 14: 65–75.
9. Dunn L, Kron T, Johnston PN, McDermott LN, Taylor ML, Callahan J, Franich RD. A programmable motion phantom for quality assurance of motion management in radiotherapy. *Australas Phys Eng Sci Med* 2012; 35: 93–100.
10. Pallotta S, Calusi S, Masi L, Talamonti C, Marrazzo L, Foggi L, Casati M, Livi L, Simontacchi G, Desideri I, Lisci R. ADAM phantom to test 4D medical imaging and dose delivery devices. *Phys Med Biol* 2019; 64: 105002.
11. Shiinoki T, Fujii F, Fujimoto K, Yuasa Y, Sera T. A novel dynamic robotic moving phantom system for patient-specific quality assurance in real-time tumor-tracking radiotherapy. *J Appl Clin Med Phys* 2020; 21: 16–28.
12. Jursinic PA, Sharma R, Reuter J. MapCHECK used for rotational IMRT measurements: step-and-shoot, TomoTherapy, RapidArc. *Med Phys* 2010; 37: 2837–2846.
13. Decabooter E, Roijen E, Martens J, Unipan M, Bosmans G, Vilches-Freixas G. Quality assurance of scanned proton beams at different gantry angles using an ionization chamber array in a rotational phantom. *Phys Med* 2022; 104: 67–74.
14. Urso P, Lorusso R, Marzoli L, Corletto D, Imperiale P, Pepe A, Bianchi L. Practical application of Octavius[®]-4D: Characteristics and criticalities for IMRT and VMAT verification. *J Appl Clin Med Phys* 2018; 19: 517–524.
15. Rinaldin G, Perna L, Agnello G, Pallazzi G, Cattaneo GM, Fiorino C, Calandrino R. Quality assurance of rapid arc treatments: performances and pre-clinical verifications of a planar detector (MapCHECK2). *Phys Med* 2014; 30: 184–190.
16. Jeevanandam P, Agnew CE, Irvine DM, McGarry CK. Improvement of off-axis SABR plan verification results by using adapted dose reconstruction algorithms for the Octavius 4D system. *Med Phys* 2018; 45: 1738–1747.
17. Stelljes TS, Harmeyer A, Reuter J, Looe HK, Chofor N, Harder D, Poppe B. Dosimetric characteristics of the novel 2D ionization chamber array OCTAVIUS Detector 1500. *Med Phys* 2015; 42: 1528–1537.
18. Sarudis S, Karlsson A, Nyman J, Bäck A. Dosimetric effects of respiratory motion during stereotactic body radiation therapy of lung tumors. *Acta Oncol* 2022; 61: 1004–1011.
19. Yoshioka S, Akino Y, Shiomi H, Hirata T, Kai N, Ogawa K, Koizumi M. Dosimetric evaluation of CyberKnife synchrony system for liver tumors with respiratory phase shifts. *Vivo* 2022; 36: 2861–2868.
20. Choi YE, Sung K, Dong KS, Shin HB, Kim HJ, Lim YK. The effect of respiratory motion in breast intensity-modulated radiation therapy: 3D-Printed dynamic phantom study. *Anticancer Res* 2023; 43: 4425–4433.
21. Gholampourkashi S, Cygler JE, Lavigne B, Heath E. Validation of 4D Monte Carlo dose calculations using a programmable deformable lung phantom. *Phys Med* 2020; 76: 16–27.
22. Grohmann C, Frenzel T, Werner R, Cremers F. Design, performance characteristics and application examples of a new 4D motion platform. *Z Med Phys* 2015; 25: 156–167.
23. Marants R, Vandervoort E, Cygler JE. Evaluation of the 4D RADPOS dosimetry system for dose and position quality assurance of CyberKnife. *Med Phys* 2018; 45: 4030–4044.
24. Gauer T, Sothmann T, Blanck O, Petersen C, Werner R. Under-reported dosimetry errors due to interplay effects during VMAT dose delivery in extreme hypofractionated stereotactic radiotherapy. *Strahlenther Onkol* 2018; 194: 570–579.
25. Sothmann T, Gauer T, Werner R. 4D dose simulation in volumetric arc therapy: accuracy and affecting parameters. *PLoS One* 2017; 12: e0172810.
26. Mastella E, Molinelli S, Pella A, Vai A, Maestri D, Vitolo V, Baroni G, Valvo F, Ciocca M. 4D strategies for lung tumors treated with hypofractionated scanning proton beam therapy: dosimetric impact and robustness to interplay effects. *Radiother Oncol* 2020; 146: 213–220.
27. Pfeiler T, Bäumer C, Engwall E, Geismar D, Spaan B, Timmermann B. Experimental validation of a 4D dose calculation routine for pencil beam scanning proton therapy. *Z Med Phys* 2018; 28: 121–133.
28. Wu QJ, Li T, Wu Q, Yin FF. Adaptive radiation therapy: technical components and clinical applications. *Cancer J* 2011; 17: 182–189.
29. Yan D, Vicini F, Wong J, Martinez A. Adaptive radiation therapy. *Phys Med Biol* 1997; 42: 123–132.